EVALUATION OF HIGH-TEMPERATURE TENSILE PROPERTIES OF HEAT-TREATED AlSi10Mg ALLOY PRODUCED BY LASER-BASED POWDER BED FUSION

*Gianluca DI EGIDIO, Alessandro MORRI, Lorella CESCHINI

Department of Industrial Engineering (DIN), Alma Mater Studiorum, University of Bologna, Bologna, Italy, EU gianluca.diegidio2 @unibo.it*

Abstract

The AlSi10Mg alloy is widely used to produce complex-shaped components by Laser-based Powder Bed Fusion (L-PBF); these parts, characterized by light structures and high specific strength, are currently employed in high-performance room temperature applications in the automotive and aerospace industries. However, it is important to increase the data concerning the high-temperature mechanical properties of the L-PBF AlSi10Mg alloy to spread its use. This study aims to fulfill the lack of knowledge by investigating the mechanical behavior at 200 °C, a representative condition of the average temperature of engine heads, of the L-PBF AlSi10Mg alloy subjected to a T5 heat treatment (artificial aging at 160 °C for 4 h) and an innovative T6 heat treatment (solubilization at 510 °C for 10 min and artificial aging at 160 °C for 6 h). The influence of high temperatures on the mechanical behavior of the L-PBF AlSi10Mg alloy was assessed by tensile tests, while microstructural and fractographic analyses were carried out to correlate the mechanical behavior of the alloy to its microstructure, and consequently explain the failure mechanisms. The ultrafine cellular microstructure, characterizing the T5 alloy, led to higher tensile strength than the homogeneous composite-like microstructure of the T6 alloy, which makes it very interesting for future application in the automotive and aerospace industries.

Keywords: Laser-based Powder Bed Fusion (L-PBF), AlSi10Mg, high temperature, mechanical properties, microstructural characterization

1.   INTRODUCTION

The Laser-based Powder Bed Fusion (L-PBF) technology is a sustainable solution to reduce the CO_2 footprint in the energy and transportation sectors through the production of complex-shaped Al components characterized by lightweight structures and high performance [1]. However, thin-walled and lattice structures introduced to reduce weight in aerodynamic components and thermal systems must be able to withstand the thermomechanical stresses caused by the severe operating conditions that occur in these applications [2].

The AlSi10Mg alloy is currently the most common Al-based alloy used in the L-PBF process to produce complex engineering parts, fitting both mechanical (high strength/weight ratio) and production requirements (good fluidity and weldability). Despite the high room-temperature properties, the progressive loss of the strengthening mechanisms in Al-Si-Mg alloys above 200 °C, due to their low thermal stability, has limited its use in the production of components, directly or indirectly exposed to high temperatures [2,3].

It is widely known that the cellular microstructure of the L-PBF AlSi10Mg alloy in the as-built (AB) condition, which consists of supersaturated α-Al phase cells embedded in a fibrous eutectic-Si network, is metastable [4-6]. Therefore, the diffusion-driven mechanisms activated by high-temperature exposure affect both the dispersed (nano-sized Si precipitates and precursors of the Mg_2Si equilibrium phase) and aggregated (eutectic Si network) strengthening phases of the AB microstructure [4]. In particular, direct aging (DA), such as the T5 heat treatment, generally promotes only the formation and coalescence of nano-sized Si precipitates and

Mg_2Si precursors phases inside the cells of the Al matrix, while the stress-relieving (SR) and the T6 solution treatment determine a complete microstructural rearrangement into a composite-like microstructure consisting of globular Si particles incorporated into the α-Al matrix [5,6].

To the best of our knowledge, few studies are currently focused on the high-temperature mechanical behavior of the L-PBF AlSi10Mg alloy. Tocci et al. [7] studied the mechanical response at 100 °C and 150 °C of the AB and T5 (100 °C and 150 °C for 10 h) alloy, describing a good mechanical response characterized by a slight decrease in tensile strength (*UTS*), no effect on yield strength (*YS*) and an increase in elongation to failure (*e*$_f$). Uzan et al. [8] described a similar trend in the SR (300 °C for 2 h) alloy subjected to high-temperature tensile tests between 25 °C and 400 °C. In particular, the material showed a significant decrease in strength properties and an increase in the *e*$_f$ values with increasing temperature, as well as a strain-hardening attitude only below 200 °C.

Considering the limited data available, this work aims to fill the gap in knowledge concerning the effects of the high-temperature exposure (200 °C) on microstructure and tensile properties of the L-PBF AlSi10Mg alloy subjected to an optimized T5 heat-treatment (hereafter T5) and a novel rapid T6 heat-treatment (hereafter T6R) [9], thus correlating the microstructural evolution induced by the high temperatures with the mechanical performance of the L-PBF alloy.

2.   MATERIAL AND METHODS

The tensile samples were machined from bars (diameter of 9 mm and height of 77 mm) produced by a SLM 500 system in approximately 30 h using a heated platform (150 °C). A bidirectional stripes scan strategy of 67° rotation between subsequent layers and a re-melted contour zone strategy at the end of each scanning was used. The process conditions and chemical composition of the samples are summarized in **Table 1** and **Table 2**, respectively.

Table 1 L-PBF process parameters

Atmosphere	Heated platform (°C)	Laser power (W)	Scan speed (mm/s)	Spot diameter (µm)	Layer thickness (µm)	Hatch distance (µm)
Argon, $O_2 < 0.2$ vol%	150	350	1150	80	50	170

Table 2 Heat treatment conditions for the L-PBF AlSi10Mg

T5 Heat Treatment	T6R Heat Treatment
Artificial aging (AA) at 160 °C for 4h, air cooling	Solution (SHT) at 510 °C for 10 min, water quenching, artificial aging (AA) at 160 °C for 6 h, air cooling

Tensile tests were carried out, according to ISO 6892-1 and ISO 6892-2, at 200 ± 5 °C and a strain rate of 3.3×10^{-3} s^{-1} on a screw testing machine equipped with a resistance furnace and a strain gauge for high temperatures, Round-dog bone samples (gauge length $L_0 = 25$ mm and gauge diameter $d_0 = 5$ mm) were used. The soaking temperature in the furnace was verified during the tensile test by employing two type K thermocouples placed close to the specimen, in the upper and lower parts of the gauge length. The test temperature (200 °C) was reached via a heating ramp of 30 min and the sample was kept at 200 °C for further 30 minutes before starting the test, to homogenize the temperature in the bulk material. The test temperature was maintained for the entire duration of the tensile test until the sample failure. The mechanical properties (*YS*, *UTS*, and *e*$_f$) were evaluated as the average of at least four samples for each investigated condition. HV_1 hardness tests were carried out on each high-temperature tensile sample after the test. The results of the high-temperature mechanical characterization were compared with those obtained at room temperature, already published by the authors in [9].

The plastic behavior of the alloy in each tensile test condition was described by Hollomon's equation (1) to study the effects of the high temperatures on the strain-hardening ability:

$$\sigma = K\varepsilon^n \tag{1}$$

where:

σ is the true plastic stress (MPa), ε is the true plastic strain, K is the strength coefficient (MPa), and n is the strain-hardening coefficient.

The strength coefficient K and the strain hardening coefficient n were evaluated according to ISO 10275:2020 standard, considering true stress-true strain data between 2% plastic strain and the percentage plastic strain at maximum force.

## 3.   RESULTS

3.1.   Tensile tests and plastic behavior

The results of tensile tests and hardness measurements at room (T5-R and T6R-R condition) and high-temperature (T5-200 and T6R-200 condition) are compared in the histograms of **Figure 1**. To gain insight into the strain-hardening behavior, the true tensile stress-strain (σ_t-$\varepsilon_{t,p}$) and the strain-hardening rate-true strain curves (θ-ε) are reported in **Figure 2a**, while the work-hardening indexes are reported in **Figure 2b**.

As expected, the high temperatures significantly affect the mechanical response of the T5 and T6R alloy. The decrease in strength properties is important: the *YS* value is reduced by approximately 45% and 50% and the *UTS* value is reduced by approximately 65% and 60% for the T5-200 and T6R-200 conditions, respectively. The loss of efficiency at high temperatures of the strengthening mechanisms, such as those induced by aggregated second phase and precipitation hardening for the T5 alloy and dispersed second phase and precipitation hardening for the T6R alloy are the main causes of the decrease in strength properties. These results are confirmed by the hardness drop of about 20% and 25% measured on the T5-200 and T6R-200 conditions, respectively. The softening of the Al matrix at 200 °C involves a decrease in the activation energy for the dislocation motion, stimulating climbing and gliding relative to pile-up phenomena [4], and therefore induces an increase in the e_f. However, this condition is observed only on the T5-200 alloy (about 45%), while the T6R-200 alloy shows an e_f value very similar to the T6R-R one. This condition can be attributable to an inhomogeneous and localized plastic deformation of the α-Al matrix that, from a macroscopic point of view, leads to a decrease in uniform deformation and a premature failure of the samples. It is more evident by analyzing the true tensile stress-strain and the strain hardening rate curves of the different conditions reported in **Figure 2a**.

The T5-R alloy fails during the strain-hardening phase and before necking. As described by Considère's criterion, necking occurs when the identity between the true tensile stress (σ) and the strain-hardening rate (θ) is reached. However, the T5-R alloy has a large gap between the θ value at failure and the *UTS* value (**Figure 2a**). This behavior of the T5-R alloy is probably due to the high dislocation density at the eutectic-Si network/Al cells interface for pile-up phenomena [10]. Conversely, the T6R-R microstructure is less effective in hindering the dislocation motion than the T5-R one and, therefore, the T6R-R alloy is more subject to necking (**Figure 2a**) [10]. The Considère's criterion confirms the achievement of localized strain by the T6R-R alloy; in fact, the condition $\sigma=\theta$ is satisfied at the theoretical necking point $\varepsilon_{\sigma=\theta} = 0.092$, which is located between the strain at the *UTS* value (ε_{UTS}) and the strain at failure (ε_f) (**Figure 2a**). The peculiar strengthening mechanisms of the T5-R and T6R-R alloys also lead to different elastoplastic behaviors and n-index values, equal to 0.26 and 0.10 respectively **(Figure 2b)**. The eutectic-Si network within the T5-R microstructure has a high pinning effect on the dislocation motion, which leads to a high dislocation density at the eutectic-Si network/α-Al cell interface by the Orowan looping mechanism and a consequent high n-index value [10]. Conversely, the large

Si particles embedded into the T6R-R microstructure are less effective in hindering the dislocation motion, thus limiting their accumulation in small areas and, consequently, the n-index value that would be achievable.

Considering the high-temperature results, for tests carried out at 200 °C, the plastic behavior completely changes. The T5-200 and the T6R-200 alloys show (i) lower n-index values than the T5-R and T6R-R ones of about 80% (**Figure 2b**) and (ii) higher necking attitude, which is described by a theoretical necking point ($\varepsilon_{\sigma=\theta}$), equal to 0.044 and 0.024, respectively (**Figure 2a**). As reported in **Figure 2a**, the $\varepsilon_{\sigma=\theta}$ value of the T5-200 alloy occurs close to the ε_f value (0.055), showing an important uniform deformation. Conversely, the T6R-200 alloy has a larger gap between the $\varepsilon_{\sigma=\theta}$ value (0.024) and the ε_f value (0.111), which highlights an important decrease in uniform deformation. The easier dislocation motion at high temperatures and the extremely low strain-hardening ability of the T6R-200 alloy influence the plastic deformation mechanisms of the alloy, increasing the necking and decreasing the e_f value [10,11].
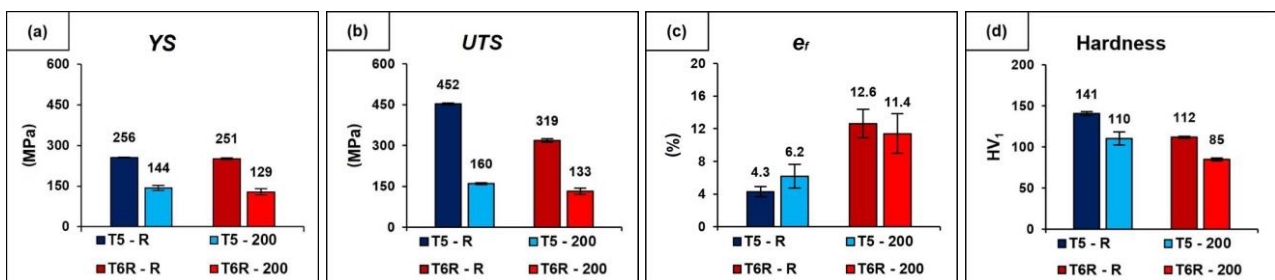
Figure 1 Tensile properties ((a) *YS*, (b) *UTS*, and (c) e_f, and (d) hardness) of the T5 and T6 alloys tested at: (i) room temperature (T5-R and T6R-R) and (ii) high temperature (T5-200 and T6R-200)
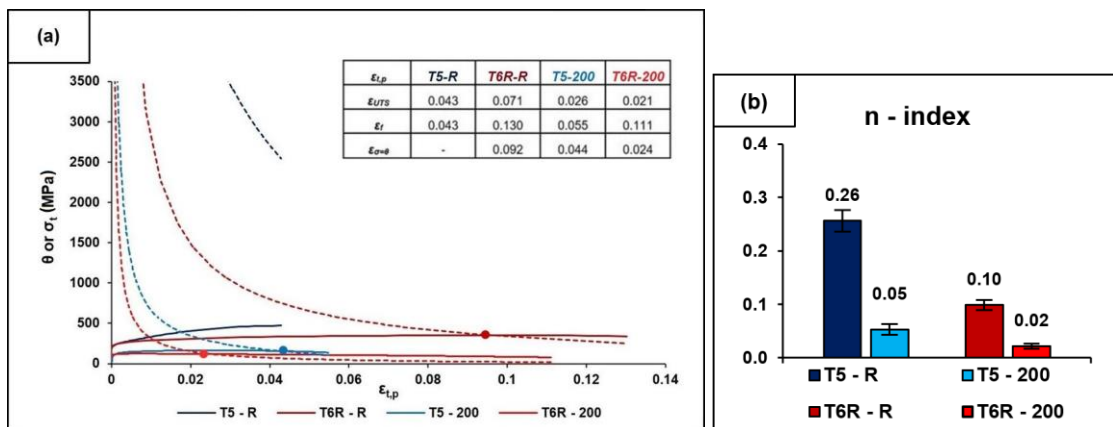
Figure 2 (a) True tensile stress-strain (solid lines) (σ_t-$\varepsilon_{t,p}$) and strain hardening rate (θ) curves (dashed lines) at room (T5-R and T6R-R) and high temperature (T5-200 and T6R-200). The table shows (i) ε_{UTS}, strain at UTS value, (ii) ε_f, strain at failure, and (iii) $\varepsilon_{\sigma=\theta}$, strain at $\sigma=\theta$ condition (dots). (b) Work-hardening index values

3.2. Microstructural and fractographic analysis

The T5-R and T6R-R alloys have microstructures very similar to those discussed in [9], which are constituted respectively by an ultrafine sub-micrometric structure of supersatured α-Al cells surrounded by a eutectic-Si network and a composite-like microstructure of Si-rich particles embedded into the α-Al matrix (**Figure 3a and 3c**), respectively. As always discussed in [9], the microstructural differences affect the mechanical response of the heat-treated alloys based on their respective strengthening mechanisms.

The change in mechanical response for the T5-200 is mainly due to the diffusion processes activated by the high temperatures which led to (i) the reduction of Si atoms in solid solution, and (ii) the coarsening of the

strengthening precipitates (nano-sized Si precipitates and precursors of the Mg_2Si equilibrium phase). Each of these changes in the strengthening mechanisms reduces the strength properties and increases the ductility, as a consequence of the reduction of the pinning effects on the dislocation motion [4]. The effects of the high temperatures on the microstructure are observable in a slight increase in Si particle size within the α-Al cells, which confirms the diffusion of Si atoms from the Al lattice, while it doesn't seem to affect the eutectic-Si network, which has a homogeneous and smooth structure, similar to the T5-R alloy (**Figure 3a** and **3b**). The high temperatures also have effects on the fracture mechanisms of the T5-200 alloy; the softening of the Al matrix, the loss of efficiency of the strengthening mechanisms, and the lower cohesion between the Al matrix/eutectic-Si network, in fact, promote higher plasticity and the formation of larger dimples at the eutectic-Si network/Al matrix interface compared to the T5-R alloy (**Figure 4a** and **4b**).

Similarly, the T6R-200 alloy undergoes a remarkable decrease in strength properties (*YS* and *UTS*), which is promoted by the rapid coarsening of the β-Mg_2Si reinforcing precipitates [4], while no-remarkable effects are observable on the Si particle size, probably due to the high thermal energy required to activate a significant Ostwald ripening phenomenon among the Si particles (**Figure 3c** and **3d**). Therefore, the drop of the e_f value is probably attributable to an inhomogeneous and localized plastic deformation induced by the softening of the Al matrix at high temperatures that leads to a decrease in the uniform deformation. This phenomenon is related to the different elastoplastic behavior of the Si particles and the Al matrix that influences the crack growth rate and the formation of dimples; in fact, the Al matrix undergoes local extensive plastic deformation around the Si particles, that is not observed in the samples tested at room temperature. Therefore, the non-homogeneous stress-state developed around the larger Si particles, which is due to the increase in local plastic flow, induces the decohesion between the Al matrix and Si particles and the formation of large dimples due to the plastic relieving of the Al matrix near the Si particles [12]. The formation of larger dimples in the T6R-200 sample compared to the T6R-R one and the presence of Si particles located at the center of the dimples confirm this interpretation (**Figure 4c** and **Figure 4d**).
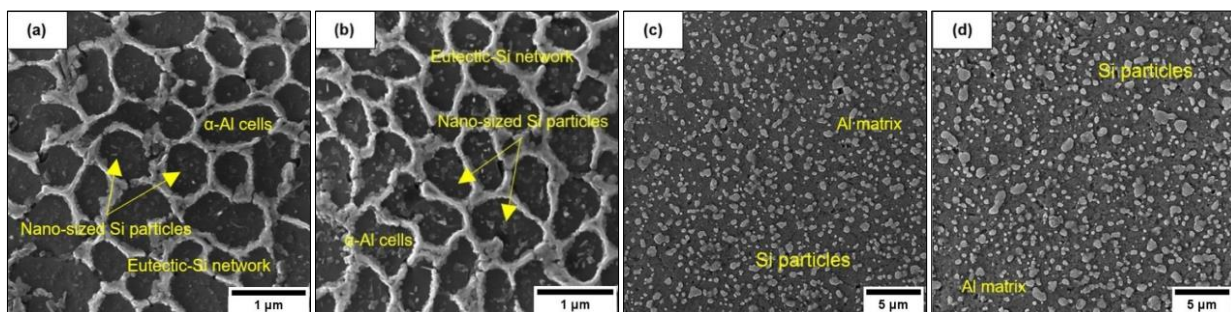
Figure 3 T5 and T6R alloy microstructures of (a,c) room temperature-tested samples (T5-R and T6R-R) and (b,d) high-temperature-tested samples (T5-200 and T6R-200)
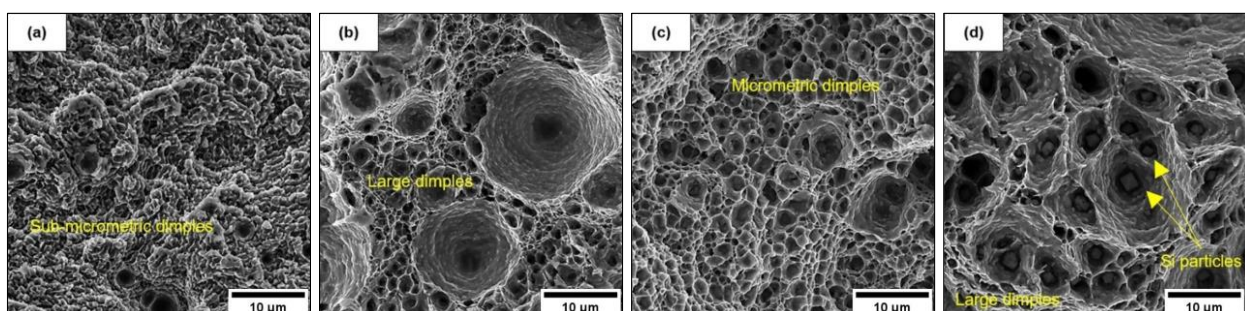
Figure 4 Fracture surfaces of T5 and T6R alloy tested at room temperature ((a) T5- R and (c) T6R-R) and at high temperature ((b) T5-200 and (d) T6R-200)

4. CONCLUSIONS

The research activity aimed at identifying the effects of high temperature (200 °C) on the microstructure and tensile properties of the L-PBF AlSi10Mg alloy, which was subjected to two different heat treatments: T5 (artificial aging at 160 °C for 4 h) and T6R (rapid solution at 510 °C for 10 min followed by artificial aging at 160 °C for 6 h). The following conclusions can be drawn:

- The T5 and T6R alloy tested at 200 °C (T5-200 and T6R-200, respectively) showed a decrease in strength properties, which was less evident in the T5-200 alloy than in the T6R-200 one. This behavior was linked to the higher efficiency at high temperatures of the strengthening mechanisms of the sub-micrometric cellular structure of the T5 alloy compared to the composite structure of the T6R one. The ductility instead increased significantly in T5-200 alloy and slightly decreased for T6R-200 one. The non-homogeneous stress state developed around the large Si particles of the T6R-200 samples led to significant necking during the high-temperature tensile test.

- At high temperatures, the T5 and T6R alloys showed a higher attitude to necking and an evident decrease in the strain-hardening ability. In particular, the T6R-200 alloy had the largest increase in necking and the lowest n-index value.

In conclusion, the T5 heat treatment seems to be more suitable for L-PBF AlSi10Mg alloy components used for applications up to 200 °C compared to the T6R one. Further investigations will be dedicated to evaluating the influence of the heat treatment also on the high-temperature fatigue behavior of the L-PBF AlSi10Mg alloy.

ACKNOWLEDGEMENTS

REFERENCES

[1] INGARAO, G., PRIARONE, P.C., DENG, Y., PARASKEVAS, D. Environmental modelling of aluminium based components manufacturing routes: Additive manufacturing versus machining versus forming. *Journal of Cleaner Production*. 2018, vol. 176, pp. 261-275.

[2] MICHI, R.A., PLOTKOWSKI, A., SHYAM, A., DEHOFF, R.R., SURESH BABU, S. Towards high-temperature applications of aluminium alloys enabled by additive manufacturing. *International Materials Reviews*. 2021, pp. 1-48.

[3] CESCHINI, L., MORRI, A., TOSCHI, S., JOHANSSON, S., SEIFFEDINE, S. Microstructural and mechanical properties characterization of heat-treated and overaged cast A354 alloy with various SDAS at room and elevated temperature. *Materials Science and Engineering: A*. 2015, vol. 648, pp. 340–349.

[4] LI, W., LI, S., LIU, J., ZHANG, A., ZHOU, Y., WEI, Q., YAN, C., SHI, Y. Effect of heat treatment on AlSi10Mg alloy fabricated by selective laser melting: Microstructure evolution, mechanical properties and fracture mechanism. *Materials Science and Engineering: A*. 2016, vol. 663, pp. 116-125.

[5] PADOVANO, E., BADINI, C., PANTARELLI, A., GILLI, F., D'AIUTO, F. A comparative study of the effects of thermal treatments on AlSi10Mg produced by laser powder bed fusion. *Journal of Alloys and Compounds*. 2020, vol. 831, Article 154822

[6] FOUSOVÁ, M., DVORSKÝ, D., MICHALCOVÁ, A., VOJTĚCH, D. Changes in the microstructure and mechanical properties of additively manufactured AlSi10Mg alloy after exposure to elevated temperatures. *Materials Characterization*. 2018, vol. 137, pp. 119-126.

[7] TOCCI, M., VARONE, A., MONTANARI, R., POLA, A. Study of high-temperature properties of AlSi10Mg alloy produced by laser-based powder bed fusion. *Materials Science Forum*. 2021, vol. 1016, pp. 1485-1491.

[8] UZAN, N.E., SHNECK, R., YEHESKEL, O., FRAGE, N. High-temperature mechanical properties of AlSi10Mg specimens fabricated by additive manufacturing using selective laser melting technologies (AM-LPBF). *Additive Manufacturing*. 2018, vol. 24, pp. 257-263.

[9] DI EGIDIO, G., CESCHINI, L., MORRI, A., MARTINI, C., MERLIN, M. A Novel T6 rapid heat treatment for AlSi10Mg alloy produced by laser-based powder bed fusion: Comparison with T5 and conventional T6 heat treatments. *Metallurgical and Materials Transactions B*. 2022, vol. 53, pp. 284–303.

[10] CHEN, B., MOON, S.K., TAO, X., BI, G., SHEN, J., UMEDA, J., KONDOH, K. Strength and strain hardening of a selective laser melted AlSi10Mg alloy. *Scripta Materialia*. 2017, vol. 141, pp. 45-49.

[11] KOCKS, U.F., MECKING, H. Physics and phenomenology of strain hardening: the FCC case. *Progress in Materials Science*. 2003, vol. 48, Issue 3, pp. 171-273.

[12] CÁCERES, C.H. A rationale for the quality index of Al-Si-Mg casting alloys. *International Journal of Cast Metals Research*. 2000, vol. 12, Issue 6, pp. 385-391.